Nano Energy 50 (2018) 710–716

Contents lists available at ScienceDirect

Nano Energy

journal homepage: www.elsevier.com/locate/nanoen

Communication

# Back-contact perovskite solar cells with honeycomb-like charge collecting electrodes

Qicheng Hou[a,b], Dorota Bacal[a,b], Askhat N. Jumabekov[b,c], Wei Li[a,b], Ziyu Wang[d,e], Xiongfeng Lin[a,b], Soon Hock Ng[f], Boer Tan[a,b], Qiaoliang Bao[d,e], Anthony S.R. Chesman[b,c,g], Yi-Bing Cheng[b,d], Udo Bach[a,b,c,g,*]

[a] Department of Chemical Engineering, Monash University, Victoria 3800, Australia
[b] ARC Centre of Excellence in Exciton Science, Monash University, Victoria 3800, Australia
[c] CSIRO Manufacturing, Clayton, Victoria 3168, Australia
[d] Department of Materials Science and Engineering, Monash University, Victoria 3800, Australia
[e] ARC Centre for Future Low-Energy Electronics Technologies, Monash University, Victoria 3800, Australia
[f] Centre for Micro-Photonics, Faculty of Science, Engineering and Technology, Swinburne University of Technology, Victoria 3122, Australia
[g] Melbourne Centre for Nanofabrication, Clayton, Victoria 3168, Australia

ARTICLE INFO

*Keywords:*
Perovskite solar cells
Back-contact
Honeycomb-shape
Photolithography
Quasi-interdigitated electrodes

ABSTRACT

Back-contact electrodes have been broadly applied to silicon photovoltaics to enhance their performance and avoid parasitic absorption from window materials and charge collection grids [1,2]. Here we introduce an innovative back-contact design for perovskite solar cells (PSCs) derived from our recently described quasi-interdigitated back-contact architecture [3]. The back contact consists of a top electrode, which has a honeycomb-like grid geometry, that is separated from the underlying planar bottom electrode by a similarly shaped insulating $Al_2O_3$ layer. This new design has higher structural robustness, as well as better defect tolerance, resulting in the highest short-circuit current (~ 16.4 mA/cm$^2$) and stabilized power output (~ 4%) for a back-contact PSC to date. The improved performance was attributed to an increased charge collecting efficiency, with photocurrent mapping revealing what electrode dimensions are required for optimum efficiency.

## 1. Introduction

The field of hybrid organic-inorganic perovskites continues to expand at a prodigious rate [4–6]. Due to their remarkable light absorbing properties, compatibility with readily scalable fabrication methods, as well as the abundance of their elemental constituents, these materials have been intensively explored as photoabsorbing layers in solar cells [5–9]. The reported photoconversion efficiencies (PCEs) of perovskite solar cells (PSCs) fabricated on a laboratory scale have increased rapidly, with a PCE exceeding 22% reported in 2016 [8,10]. These record efficiencies have been achieved using a conventional layered architecture, in which the thin perovskite film is sandwiched in between the hole/electron collection layers and the electrodes. However, this device configuration poses a number of inherent problems during fabrication, namely the risk of pin holes in the perovskite thin film causing shorting between the electrodes, and the deposition of the top contact damaging the chemically sensitive perovskite layer.

These issues can be avoided by using a back-contact (BC) architecture, in which both the cathode and anode are positioned on one side of the photoabsorber layer. The back-contact architecture was first realized with interdigitated back-contact (IBC) silicon solar cells, and is now widely employed in commercial c-Si solar cells, with an efficiency of 21% achieved as early as 1985 [1,2]. Although this device configuration has also been employed in dye-sensitized solar cells (DSSCs) that achieved PCEs of 3.6% [11] and 4.6% [12], experimental [3,13–16] studies have only recently demonstrated back-contact PSCs, with a stabilized power output of 3.2% reported [3]. Despite the relatively low efficiencies reported to date, simulations predict the device structure holds immense potential for PSCs, with theoretical calculations predicting PCEs of over 22% [17]. As the perovskite is the final layer to be deposited during device fabrication, any losses through parasitic light absorption by the top contact are avoided and damage to the photoabsorber during subsequent fabrication steps is eliminated. Therefore, the nature of BC electrodes also favors their application to tandem solar cells, where the photoabsorbing layers can convert incident photons more efficiently due to less parasitic absorption caused

* Corresponding author at: Department of Chemical Engineering, Monash University, Victoria 3800, Australia.
*E-mail address:* udo.bach@monash.edu (U. Bach).

https://doi.org/10.1016/j.nanoen.2018.06.006
Received 28 April 2018; Received in revised form 29 May 2018; Accepted 3 June 2018
Available online 05 June 2018
2211-2855/ 

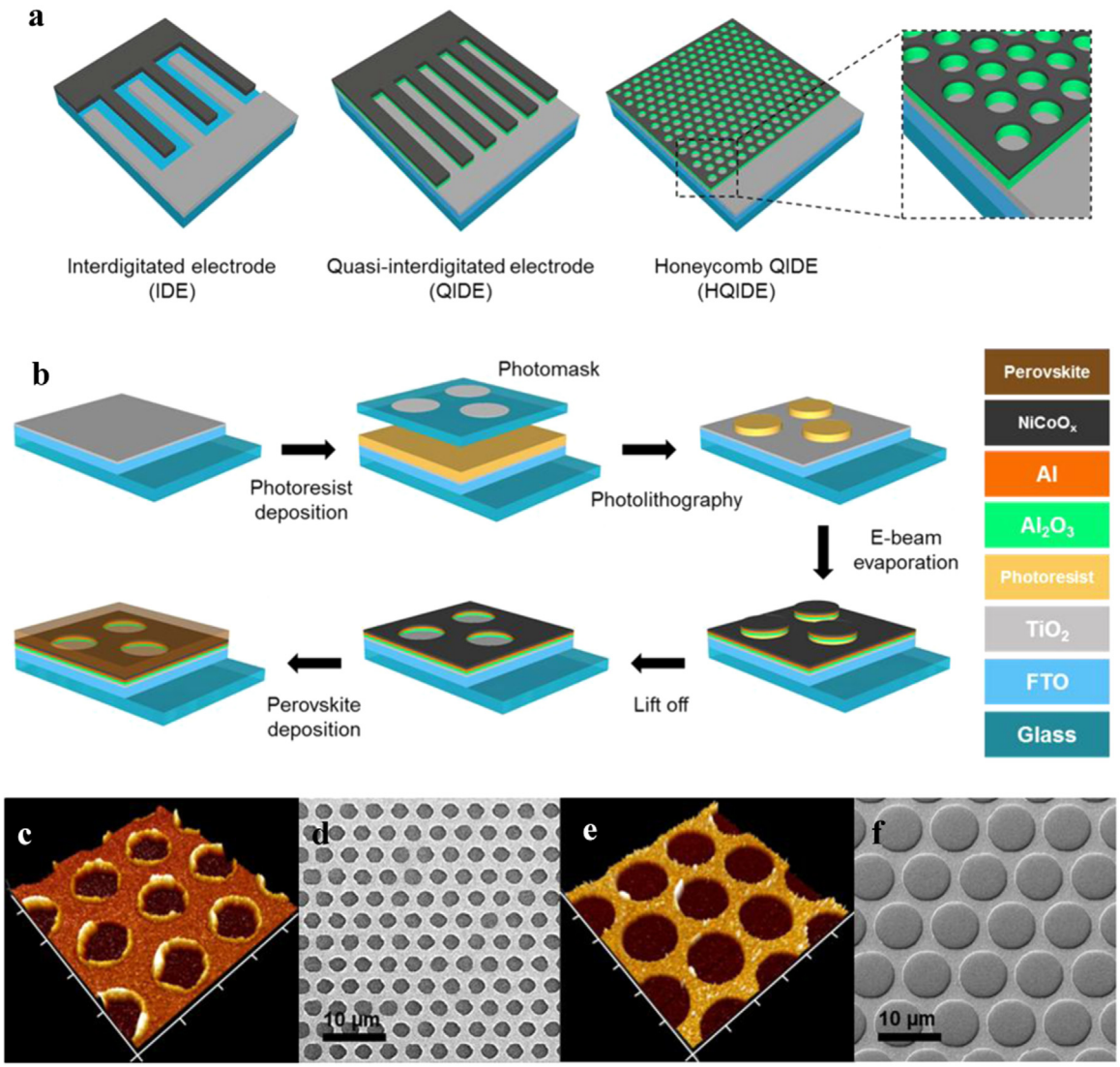


**Fig. 1.** a) Schematic diagram of a variety of electrode architectures employed in back-contact PSCs; b) Flow chart of the HQIDE device fabrication process; c and e) AFM images of the S-HQIDE with the axis unit scale as 2.5 μm and L-HQIDE with the axis unit scale as 5 μm; d and f) SEM images of the surface of an S-HQIDE and an L-HQIDE.

by electrode and charge extraction layers [8,18,19]. Additionally, in contrast to conventional PSCs with a layered architecture, BC-PSCs feature a fully exposed perovskite surface, which opens a window for the in-situ study of perovskite surface treatment effects and their influence on device performance [2,20].

Despite these advantages, BC architectures present different challenges during fabrication. To date, the majority of BC solar cells use interdigitated electrodes (IDE), in which the cathode and anode take the form of separate, yet closely spaced, interdigitated fingers (Fig. 1a) [11,13]. Any defects that arise during fabrication via photolithography can cause contact between the two electrodes, which ultimately leads to device failure due to catastrophic shorting [3]. This problem was overcome by developing the quasi-interdigitated electrode (QIDE), in which the top finger electrode is separated by an insulator layer from the planar bottom electrode (Fig. 1a) [3]. Since the two electrodes are no longer coplanar, defects in the electrode fingers will not cause short-circuiting. However, a break in the fingers of the electrode will still isolate a portion of the top contact, decreasing the charge collection area and consequently reducing the efficiency of the solar cell. Our group has recently taken first steps to replace the defect-prone finger structure with a coplanar architecture featuring a partially perforated top electrode, however control of the regularity of the hole pattern was limited and efficiencies of devices were low [14].

In this communication, we address this issue through the development of a honeycomb quasi-interdigitated electrode (HQIDE), in which the top electrode adopts a honeycomb-like morphology. This back-contact architecture not only preserves the benefit of decreased short-circuiting observed in QIDEs, but also substantially increases defect tolerance, as any discontinuity in the electrode does not result in isolation.

## 2. Results and discussion

The structure of a PSC incorporating a HQIDE is shown in Fig. 1b. Under illumination, charge carriers are generated in the perovskite photoabsorber layer, with the $TiO_2$ layer and the $NiCoO_x$ grid acting as the electron and hole transport materials, respectively. The $Al_2O_3$ layer insulates the top contact from the underlying $TiO_2$, with the Al layer enhancing the conductivity of the NiCo layer in the hole-collecting electrode.

The HQIDE is fabricated through a series of photolithography and e-beam evaporation steps (Fig. 1b). Briefly, photolithography was used to

generate a photoresist negative of the honeycomb-like grid pattern on the $TiO_2$-coated FTO glass. $Al_2O_3$, Al and NiCo were evaporated sequentially onto the substrate, followed by lift-off of the photoresist, yielding the top electrode grid (optical images can be found in Supporting information, Fig. S1). Finally, the substrate was annealed at 300 °C for 15 min to oxidize the surface of the NiCo layer. The oxidation process resulted in a work-function increase of 230 meV as verified by photoelectron spectroscopy in air (PESA) measurements (see Supporting information, Fig. S2), indirectly confirming the formation of a $NiCoO_x$ layer. Device fabrication was completed by depositing a $CH_3NH_3PbI_3$ thin-film with a gas-assisted spin-coating method [21]. Complete details of the fabrication procedure can be found in Section 4.

Atomic force microscopy (AFM) and scanning electron microscopy (SEM) were used to investigate the topology of the HQIDE prior to the deposition of the perovskite layer. Two types of HQIDE were fabricated over the course of this study; a HQIDE with smaller exposed areas of $TiO_2$ (S-HQIDE) and a HQIDE with larger exposed areas of $TiO_2$ (L-HQIDE). The diameter of the circular gaps in the top electrode for S-HQIDE is about 2.7 µm, with a 1.3 µm spacing between the edges (Fig. 1c, d), while the L-HQIDE had circular gaps and spacing between the edges of around 8.0 µm and 1.5 µm, respectively (Fig. 1e, f).

The photovoltaic performances of PSCs employing HQIDE electrodes were measured via photocurrent (PC) density – voltage characterization under AM1.5 G simulated sunlight under reverse (from open circuit voltage ($V_{oc}$) to 0 V) and forward scan (from 0 V to $V_{oc}$) conditions (see Fig. 2a). The corresponding values of $V_{oc}$, short circuit current ($J_{sc}$), fill factor (FF) and power conversion efficiency (PCE) for the best performing devices and a batch of 6 cells are given in Table 1. Generally, all BC-PSCs showed strong hysteresis, while maximum power point (MPP) tracking revealed stabilized power outputs of 4.0% and 0.72% for the best performing S-HQIDE and L-HQIDE BC-PSCs, respectively (Fig. 2b). This suggests that the performance values obtained under forward scan conditions are a good indication of the BC-PSCs actual power output under operation. Compared to BC-PSCs incorporating IDEs or QIDEs [3,16], our device (S-HQIDE) demonstrates the highest stabilized PCE and photocurrent ever reported for a BC-PSC ($J_{sc}$ = 16.4 mA/cm$^2$ under reverse scan).

As previously postulated [16], the electrode dimensions have a dramatic impact on device performance. Reducing the centre-to-centre pitch of our honeycomb-electrode structure from 9.5 µm (L-HQIDE) to 4 µm (S-HQIDE) increased the stabilized power output by a factor of 5.7 and the stabilized photocurrent density at the maximum power point by a factor of 4.5 (see Supporting information, Fig. S3). The pitch reduction also resulted in a significant FF increase, indicating that charge transport in PSCs with micron-sized electrode features is limited by the ohmic resistance of the perovskite layer itself.

The existence of grain boundaries in $CH_3NH_3PbI_3$ films has been reported to have a detrimental effect on the open circuit voltage of PSCs [22], and is potentially problematic in BC-PSCs where photogenerated charges typically have to travel several microns before reaching their respective collection electrodes. We have therefore investigated the morphology of perovskite thin films grown on FTO/$TiO_2$ ($TiO_2$), FTO/$Al_2O_3$/Al/NiCo/$NiCoO_x$ ($NiCoO_x$) and complete HQIDEs (Fig. 3). SEM and AFM images reveal that while the perovskite grains have an average size of 450 nm when deposited onto $TiO_2$, they decrease in size to 320 nm on $NiCoO_x$, and shrink further to 250 nm on the HQIDE. This may be a result of the different surface energies of $TiO_2$ and $NiCoO_x$ layers, causing a difference in the wettability of the perovskite precursor solution on the surfaces, as confirmed by contact angle measurements in Fig. S4 (see Supporting information). The poorer wettability of $NiCoO_x$ compared with $TiO_2$ resulted in the decrease of the perovskite grain size [23–25]. Finally, the smallest grain size found on the HQIDE may be attributed to its topological structure, which provide a significant number of nucleation sites during thin film formation.

Photocurrent mapping was used to determine the influence of electrode dimensions on the HQIDE's photovoltaic performance (Fig. 4). The photocurrent maps were obtained with a confocal microscope setup, and normalized relative to the average photocurrent across the scan area in order to facilitate a direct comparison of the uniformity of the photocurrent generation within the two different structures. The photocurrent variability is significantly larger for L-HQIDEs than S-HQIDEs, which is in general agreement with the higher photocurrent densities measured for S-HQIDEs. For photocurrent generation to be highest two requirements must be met; the location of light absorption needs to be above a $TiO_2$ collection electrode and within about 1 µm of a hole collecting $NiCoO_x$ electrode. Regions of perovskite that are long distances from an electrode for at least one of the two carrier types, such as the centre of the exposed circular $TiO_2$ electrode, exhibit low PCs. Although there are differing opinions on the diffusion lengths of free charge carriers in $CH_3NH_3PbI_3$ [26–28], the locations of PC maxima in Fig. 4b and d may suggest that holes can diffuse a longer distance before recombining, compared with electrons in both S-HQIDE and L-HQIDE, which was in line with observations from the charge mobility studies of $CH_3NH_3PbI_3$ [29,30].

## 3. Conclusion

In summary, we have presented a novel electrode design for back-contact solar cells. By applying this new architecture to the field of back-contact PSCs we were able to fabricate solar cells with unprecedented photocurrent densities above 16 mA/cm$^2$ under solar illumination. This is significantly higher than previously reported

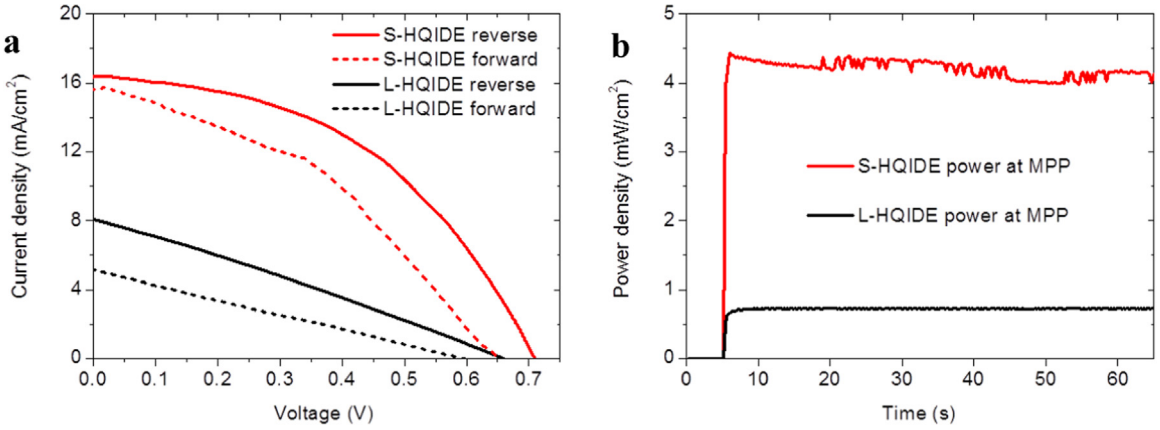


**Fig. 2.** a) Photocurrent density–voltage curves of the best-performing PSCs based on S-HQIDE and L-HQIDE recorded under different scan directions under simulated AM1.5 G (1000 W/m$^2$) irradiation; b) Time dependent measurements of stabilized power density at the maximum power point for the best-performing S-HQIDE and L-HQIDE PSCs.

**Table 1**
Photovoltaic performances of BC-PSCs based on S-HQIDE and L-HQIDE under reverse and forward scanning conditions and simulated AM1.5 G (1000 W/m$^2$) irradiation. Scan speed: 100 mV/s.

| Champion | Scan | $V_{oc}$ [V] | $J_{sc}$ [mA/cm$^2$] | FF [%] | PCE [%] |
|---|---|---|---|---|---|
| S-HQIDE | Reverse | 0.70 | 16.4 | 46.9 | 5.39 |
| | Forward | 0.64 | 15.6 | 40.1 | 4.01 |
| L-HQIDE | Reverse | 0.66 | 8.09 | 27.4 | 1.46 |
| | Forward | 0.60 | 5.13 | 24.7 | 0.76 |
| **Statistics** | | | | | |
| S-HQIDE | Reverse | 0.71 ± 0.02 | 15.3 ± 1.37 | 44.4 ± 2.97 | 4.87 ± 0.68 |
| | Forward | 0.65 ± 0.02 | 14.5 ± 1.46 | 37.0 ± 3.97 | 3.52 ± 0.67 |
| L-HQIDE | Reverse | 0.64 ± 0.03 | 7.04 ± 1.35 | 27.1 ± 0.67 | 1.23 ± 0.30 |
| | Forward | 0.57 ± 0.03 | 4.40 ± 0.97 | 24.0 ± 1.36 | 0.62 ± 0.18 |

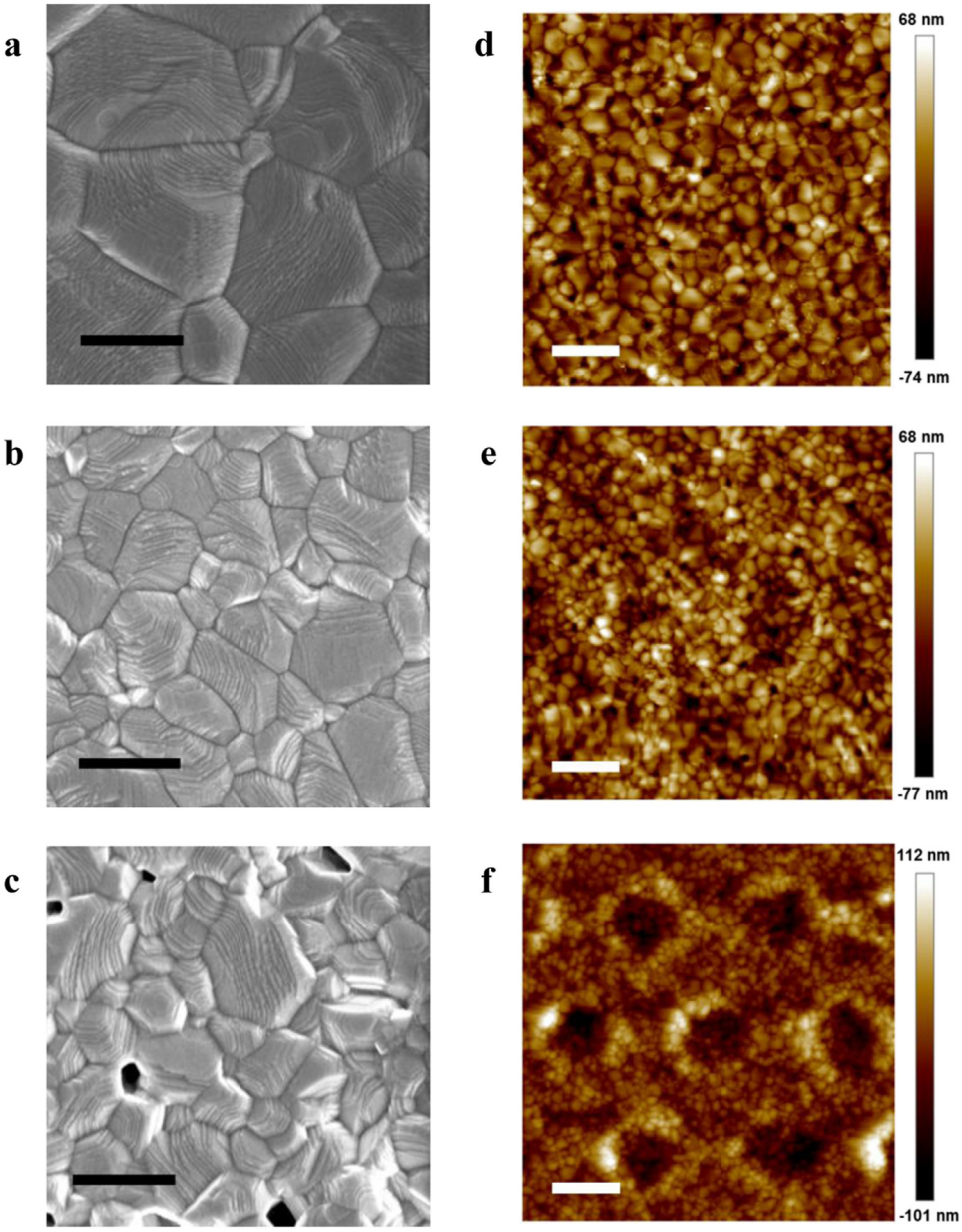


**Fig. 3.** a–c) SEM images of perovskite films deposited on FTO/$TiO_2$, FTO/$Al_2O_3$/Al/NiCo/$NiCoO_x$ and FTO/$TiO_2$/HQIDE, respectively (scale bars: 500 nm); d–f) AFM images of perovskite films deposited on FTO/$TiO_2$, FTO/$Al_2O_3$/Al/ NiCo/$NiCoO_x$ and FTO/$TiO_2$/HQIDE, respectively (scale bars: 2 μm).

photocurrents [3,14–16], proving the superior charge collection efficiency of this novel electrode structure. The application of the HQIDE design, along with the further miniaturization of the electrode features, optimization of the contacts, and the formation of perovskite films with higher crystallinity, will help to close the present efficiency gap between back-contact and conventional sandwich-structure PSCs.

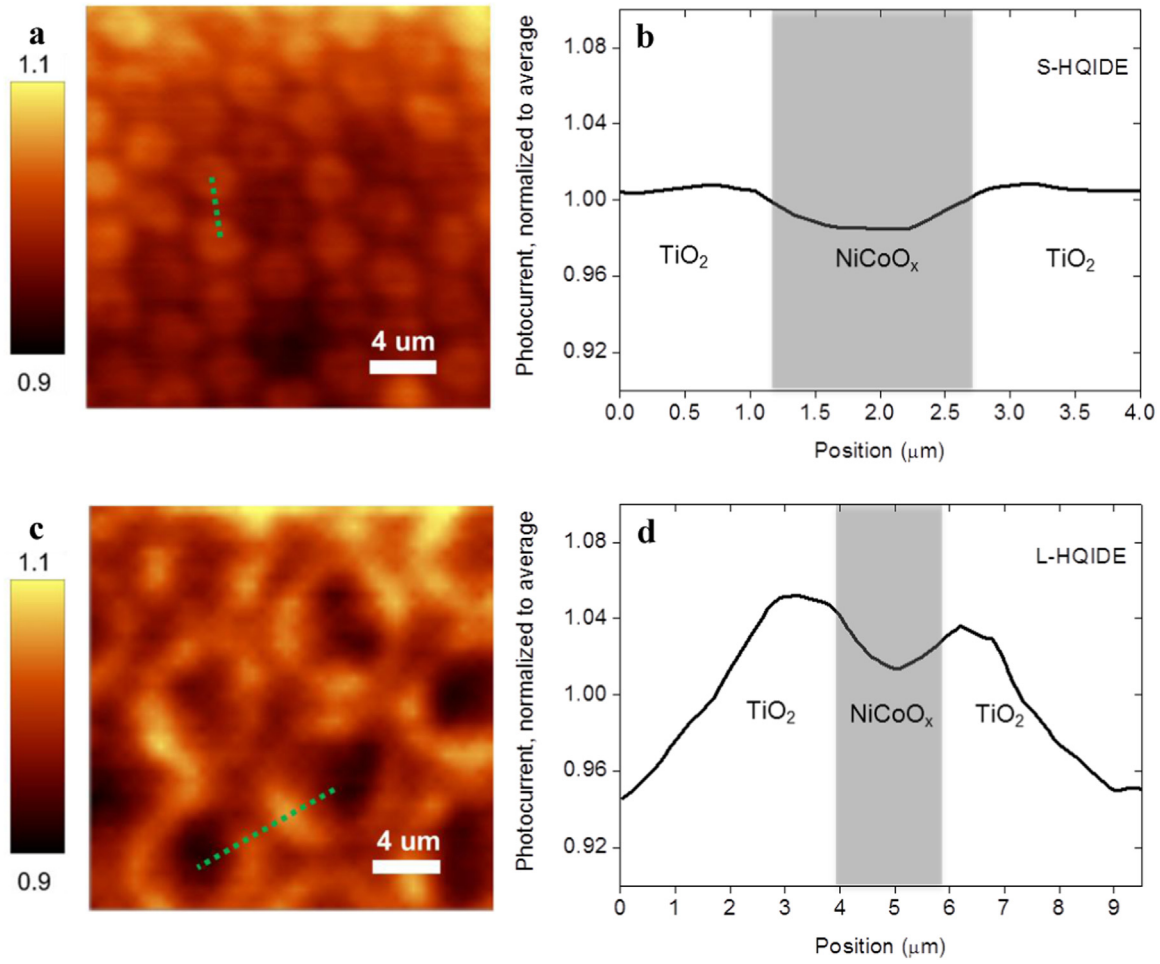


**Fig. 4.** PC maps (with photocurrent normalized to average) of perovskite solar cells based on a) S-HQIDE, c) L-HQIDE; b and d) normalized photocurrent profiles for the devices with S-HQIDE and L-HQIDE along the green dashed lines in a) and c).

## 4. Experimental section

### 4.1. Materials

Unless specified otherwise, all materials for perovskite precursor preparation were purchased from either Alfa Aesar or Sigma-Aldrich and used as received. AZ1512HS photoresist and AZ726MF developer were purchased from MicroChemicals. FTO-coated glass was purchased from Kaivo with a sheet resistance of less than 15 Ω/sq.

### 4.2. Electrode fabrication

FTO-coated glass substrates (10 cm × 10 cm) were cleaned by sequentially sonicating for 15 min in baths of Hellmanex®III solution, water, and ethanol. After cleaning, the FTO-coated glass was placed on a hotplate and heated to 500 °C, at which point a diluted 75 wt% titanium-diisopropoxide bis(acetylacetonate) (75 wt% TAA) in isopropanol (IPA) solution (75 wt% TAA:IPA = 1:19 v/v) was deposited by spray coating, resulting in the formation of a uniform $TiO_2$ thin film. The temperature of the substrate was maintained at 500 °C for 10 min, and the substrate was then allowed to cool down on the hotplate. The substrate was subsequently cut into ~ 2.5 cm × 2.5 cm squares prior to photolithography. An adhesion promoter, hexamethyldisilazane (HMDS), was spin-coated at 7000 rpm for 30 s on the FTO/$TiO_2$ substrate, which was subsequently baked at 110 °C for 1 min. The AZ1512HS photoresist was then spin-coated using the same deposition conditions, followed by annealing at 110 °C for 2 min. The sample was then mounted to a photomask and placed on the holder of a UV flood light source (UV Exposure System from ABM-USA, power 10.4 mW/cm$^2$ at 365 nm) for exposure. The substrate was exposed to the light source for 7.5 s to develop the pattern. Subsequently, the exposed sample was immersed into a solution of AZ726MF developer in water (2:1 v/v) for ~ 25 s to selectively remove the part of the photoresist that had been exposed to UV light. An e-beam evaporator was used to sequentially deposit $Al_2O_3$ (135 nm), Al (30 nm) and Ni-Co (50 nm, Ni:Co ratio of 1:1) onto the substrates. The deposition rates were ~ 0.6 Å/s, 0.5 Å/s and 0.5 Å/s, respectively. After the deposition was completed, the samples were immersed in acetone to lift off the layers that were deposited onto the photoresist. Samples were then sequentially sonicated for 10 min in baths of IPA and DI water.

### 4.3. Device fabrication

Before perovskite thin-film deposition, the electrodes were annealed at 300 °C for 15 min to oxidize the surface of the NiCo to $NiCoO_x$. A $CH_3NH_3PbI_3$ precursor solution was prepared by dissolving $CH_3NH_3I$ and $PbI_2$ in dimethylformamide (DMF) at 50 wt% in a 1:1 M ratio. The perovskite precursor solution (~ 50 μL) was spin coated onto the electrodes at 6500 rpm for 30 s, with an $N_2$ stream introduced after 3 s of spin-coating to assist in uniform thin-film formation [21]. The samples were then annealed at 100 °C for 10 min.

### 4.4. Characterization

Surface SEM images were obtained using a Magellan scanning

electron microscope operated at 2 or 5 kV. A cross-section of the sample was prepared by a Helios NanoLab 600 Focus Ion Beam system. AFM measurements were obtained with a Dimension Icon (Veeco) in air using tapping mode. Water contact angle data were collected on a PGx portable contact angle measurement meter using a 1.5 μL droplet at equilibrium. Reported values are an average of 3 measurements. The work functions of the samples were measured using a Riken Keiki Photoelectron Spectrometer (Model AC-2) with a UV intensity of 20 nW. The data is fitted as the square root (n = 2) of the emission yield for NiCo, and as the cube root (n = 3) of the emission yield for $NiCoO_x$. The J-V characteristics of the devices were measured in an inert atmosphere with a computer-controlled Keithley 2400 Sourcemeter. A 150 W Xenon lamp (Newport) coupled with an AM 1.5 G solar spectrum filter was used as the light source. Light was passed through a quartz window of the glove box and the intensity was calibrated and monitored using a secondary reference photodiode (Hamamatsu S1133, with KG-5 filter, 2.8 × 2.4 mm photosensitive area), which was calibrated by a certified reference cell (PVMeasurements, certified by NREL) under 1000 $W/m^2$ AM 1.5 G illumination from an Oriel AAA solar simulator fitted with a 1000 W Xenon lamp. Devices were measured at the same position as the secondary reference cell. Photocurrent mapping was performed on a custom-built setup based on a modified WiTec Alpha 300 R confocal Raman/PL microscope operating in reflection mode. The system used a Nd:YAG diode laser (wavelength: 532 nm) chopped with a C995 optical chopper (Terahertz Technologies Inc.). Amplifier settings were chosen to achieve the synchronous detection of the PC signal. To acquire a two-dimensional spectral map, the device under testing was moved with the X-Y piezo stage of the microscope. The photocurrent image was acquired by recording the drain current at zero drain–source bias while a focused green laser (spot size: ≈ 300 nm, power: 2 μW) was scanned in a defined area (20 × 20 μm).

## Acknowledgements

This work was financially supported by the Australian Government through the Australian Renewable Energy Agency (ARENA), the Australian Centre for Advanced Photovoltaics (ACAP), Australian Research Council (ARC) discovery project (DP160104575), and the ARC Centre of Excellence in Exciton Science (ACEX) (CE170100026). This work was performed in part at the Melbourne Centre for Nanofabrication (MCN) in the Victorian Node of the Australian National Fabrication Facility (ANFF). The authors acknowledge use of facilities within the Monash Centre for Electron Microscopy (MCEM). The authors thank Dr. Ricky T. Tjeung, Dr. Yang Choon Lim and Dr. Abu Sadek for their assistance with photolithography and electron-beam evaporation.

## Appendix A. Supporting information

Supplementary data associated with this article can be found in the online version at http://dx.doi.org/10.1016/j.nanoen.2018.06.006.

## References

[1] E. Van Kerschaver, G. Beaucarne, Prog. Photovolt. Res. Appl. 14 (2006) 107–123.
[2] P.J. Verlinden, R.M. Swanson, R.A. Crane, Prog. Photovolt. Res. Appl. 2 (1994) 143–152.
[3] A.N. Jumabekov, E. Della Gaspera, Z.-Q. Xu, A.S.R. Chesman, J. van Embden, S.A. Bonke, Q. Bao, D. Vak, U. Bach, J. Mater. Chem. C 4 (2016) 3125–3130.
[4] M.A. Green, Nat. Energy 1 (2016) 15015.
[5] R.F. Service, Science 344 (2014) 458.
[6] G. Hodes, Science 342 (2013) 317–318.
[7] S.D. Stranks, H.J. Snaith, Nat. Nanotechnol. 10 (2015) 391–402.
[8] N.N. Lal, Y. Dkhissi, W. Li, Q. Hou, Y.B. Cheng, U. Bach, Adv. Energy Mater. 7 (2017) 1–18.
[9] C. Roldan-Carmona, O. Malinkiewicz, A. Soriano, G. Minguez Espallargas, A. Garcia, P. Reinecke, T. Kroyer, M.I. Dar, M.K. Nazeeruddin, H.J. Bolink, Energy Environ. Sci. 7 (2014) 994–997.
[10] NREL Efficiency Chart, 2018.
[11] D. Fu, X. Li Zhang, R.L. Barber, U. Bach, Adv. Mater. 22 (2010) 4270–4274.
[12] D. Fu, P. Lay, U. Bach, Energy Environ. Sci. 6 (2013) 824–829.
[13] L.M. Pazos-Outón, M. Szumilo, R. Lamboll, J.M. Richter, M. Crespo-Quesada, M. Abdi-Jalebi, H.J. Beeson, M. Vrućinić, M. Alsari, H.J. Snaith, B. Ehrler, R.H. Friend, F. Deschler, Science 351 (2016) 1430–1433.
[14] A.N. Jumabekov, J.A. Lloyd, D.M. Bacal, U. Bach, A.S.R. Chesman, ACS Appl. Energy Mater. 1 (2018) 1077–1082.
[15] Z. Hu, G. Kapil, H. Shimazaki, S.S. Pandey, T. Ma, S. Hayase, J. Phys. Chem. C 121 (2017) 4214–4219.
[16] X. Lin, A.N. Jumabekov, N.N. Lal, A.R. Pascoe, D.E. Gómez, N.W. Duffy, A.S.R. Chesman, K. Sears, M. Fournier, Y. Zhang, Q. Bao, Y.B. Cheng, L. Spiccia, U. Bach, Nat. Commun. 8 (2017) 613.
[17] T. Ma, Q. Song, D. Tadaki, M. Niwano, A. Hirano-Iwata, ACS Appl. Energy Mater. 1 (2018) 970–975.
[18] G.W.P. Adhyaksa, E. Johlin, E.C. Garnett, Nano Lett. 17 (2017) 5206–5212.
[19] H. Savin, P. Repo, G. von Gastrow, P. Ortega, E. Calle, M. Garín, R. Alcubilla, Nat. Nanotechnol. 10 (2015) 624–628.
[20] N.K. Noel, A. Abate, S.D. Stranks, E.S. Parrott, V.M. Burlakov, A. Goriely, H.J. Snaith, ACS Nano 8 (2014) 9815–9821.
[21] F. Huang, Y. Dkhissi, W. Huang, M. Xiao, I. Benesperi, S. Rubanov, Y. Zhu, X. Lin, L. Jiang, Y. Zhou, A. Gray-Weale, J. Etheridge, C.R. McNeill, R.A. Caruso, U. Bach, L. Spiccia, Y.-B. Cheng, Nano Energy 10 (2014) 10–18.
[22] W. Nie, H. Tsai, R. Asadpour, J. Blancon, A.J. Neukirch, G. Gupta, J.J. Crochet, M. Chhowalla, S. Tretiak, M.A. Alam, H. Wang, A.D. Mohite, Science 347 (2015) 522–525.
[23] J.Y. Jeng, K.C. Chen, T.Y. Chiang, P.Y. Lin, T. Da Tsai, Y.C. Chang, T.F. Guo, P. Chen, T.C. Wen, Y.J. Hsu, Adv. Mater. 26 (2014) 4107–4113.
[24] D. Zhao, M. Sexton, H.Y. Park, G. Baure, J.C. Nino, F. So, Adv. Energy Mater. 5 (2015) 1–5.
[25] J. Burschka, N. Pellet, S.-J. Moon, R. Humphry-Baker, P. Gao, M.K. Nazeeruddin, M. Grätzel, Nature 499 (2013) 316–319.
[26] G. Xing, N. Mathews, S. Sun, S.S. Lim, Y.M. Lam, M. Graïzel, S. Mhaisalkar, T.C. Sum, Science 342 (2013) 344–347.
[27] S.D. Stranks, G.E. Eperon, G. Grancini, C. Menelaou, M.J.P. Alcocer, T. Leijtens, L.M. Herz, A. Petrozza, H.J. Snaith, Science 342 (2013) 341–344.
[28] N.G. Park, Mater. Today 18 (2015) 65–72.
[29] E. Edri, S. Kirmayer, A. Henning, S. Mukhopadhyay, K. Gartsman, Y. Rosenwaks, G. Hodes, D. Cahen, Nano Lett. 14 (2014) 1000–1004.
[30] Y. Li, W. Yan, Y. Li, S. Wang, W. Wang, Z. Bian, L. Xiao, Q. Gong, Sci. Rep. 5 (2015) 1–8.

**Qicheng Hou** is a Ph.D. candidate in the Department of Chemical Engineering, Monash University. He received his B.E. (Honors) from Monash University (Australia) and Central South University (China) in 2014. He is working with Prof. Bach on perovskite/silicon tandem solar cells and back-contact perovskite solar cells.

**Dorota Malwina Bacal** is a Ph.D. candidate in Chemical Engineering at Monash University. She completed both her B.Sc. and M.Sc. in Applied Physics Engineering at the University of Rzeszow (Poland), where she studied silicon and CdS/CdTe solar cells. Her Ph.D. research topic focuses on back-contact perovskite solar cells, in-situ measurements of the photoactive material and antireflective coatings. Dorota is directing her scientific research towards commercialization. Her affiliation with CSIRO has enabled her to start working in the Flexible Electronics Laboratory where she is developing back contact perovskite solar cells on a flexible substrate.

**Askhat N. Jumabekov** has recently completed his post-doctoral research fellowship at the Commonwealth Scientific and Industrial Research Organisation (CSIRO). He received his Ph.D. degree at the Ludwig Maximilian University of Munich in Germany in Physical Chemistry. Askhat's research focus is on device architecture and the design of hybrid organic-inorganic perovskite solar cells.

**Wei Li** is currently a postdoctoral research fellow in the Department of Chemical Engineering, Monash University. He received his Bachelor and Master's degrees from the Department of Materials Science and Engineering, Wuhan University of Technology in 2006 and 2009, respectively. In 2013, he obtained his Ph.D. from the School of Photovoltaic and Renewable Energy Engineering, The University of New South Wales. His current research interest focuses on high-efficiency perovskite solar cells and microstructure characterizations for photovoltaic materials.

**Ziyu Wang** is currently a Ph.D. candidate in the Department of Materials Science and Engineering, Monash University. He received his B.S. degree in Materials Science and Engineering from Monash University in 2015. His research focuses on low-dimensional perovskites, and electronic and photonic applications.

**Xiongfeng Lin** received his bachelor's degree from Monash University. Currently, he is a Ph.D. candidate in the Department of Chemical Engineering supervised by Prof. Udo Bach. His research interests are interfacial modification and back-contact perovskite photovoltaic devices.

**Soon Hock** is a SIEF STEM + Business Fellow at Swinburne University of Technology. He completed his B.Sc. and B.Eng. at Monash University, where he also completed his Ph.D. in 2016, with a focus on lithography and the self-assembly of nanoparticles. He began working at the Melbourne Centre for Nanofabrication as a Process Engineer in the latter half of 2016 before perusing post-doctoral research in the Centre for Micro-Photonics at Swinburne University of Technology in early 2017. His interests include the self-assembly of nanoparticles in lithographically defined templates, PVD and RIE of nanostructured thin films and, recently, energetic materials.

**Boer Tan** is currently a Ph.D. student in Chemical Engineering in Professor Udo Bach's group at Monash University. She received her B.S. Degree in Materials Science and Engineering from Monash University and Central South University in China in December 2015. Her research focuses on the high efficiency and high stability perovskite solar cells.

**Qiaoliang Bao** received his B.A. (2000) and M.E. (2003) degrees in Materials Science and Engineering from Wuhan University of Technology (China). He obtained his Ph.D. degree (2007) in Materials Physics and Chemistry from Wuhan University (China). He worked as a postdoctoral fellow at Nanyang Technological University and National University of Singapore from 2007 to 2012. He is currently an Associate Professor in the Department of Materials Science and Engineering, Monash University. His research interests include synthesis and optical characterization of two-dimensional materials, as well as their incorporation into photonic and optoelectronic devices. He has authored or co-authored more than 150 refereed journal articles with more than 15,000 total citations and an h-index of 50.

**Anthony Chesman** is a Senior Research Scientist at the Commonwealth Scientific and Industrial Research Organisation (CSIRO) and is the Team Leader of the Nanomaterials and Devices Team. Anthony is also a Partner Investigator in the Australian Research Council's Centre of Excellence in Exciton Science and is a Technology Fellow Ambassador at the Melbourne Centre for Nanofabrication (MCN). Anthony's research interests focus on the use of nanostructured materials for novel photocatalysts and new electrode structures for perovskite solar cells.

**Yi-Bing Cheng** is a Thousand Talents professor at Wuhan University of Technology, China and an Adjunct Professor in the Faculty of Engineering, Monash University, Australia. He completed his undergraduate (1978) and Master (1983) studies at Wuhan University of Technology, China and received a Ph.D. degree from University of Newcastle-upon-Tyne, U.K. in 1989. He was an academic staff at Monash University between October 1991 and March 2018. He specializes in inorganic materials. Perovskite solar cells are his current research interest.

**Udo Bach** is a full professor at Monash University, the Deputy Director of the ARC Centre of Excellence in Exciton Science and an ANFF-VIC Technology Fellow at the Melbourne Centre of Nanofabrication (MCN). He received his Ph.D. from the Swiss Federal Institute of Technology (EPFL, Switzerland) working in the research group of Prof Michael Grätzel. Subsequently he worked for 3 years in a technology start-up company in Dublin (Ireland) and spent 15 months as a postdoc in the group of Prof. Paul Alivisatos in UC Berkeley (USA) before moving to Monash University in November 2005 to establish his own research group. Prof Bach has a strong background in the area of photovoltaics and nanofabrication. He is involved in fundamental and applied research in the area of perovskite, dye-sensitized and plasmonic solar cells. He has additional research activities in the area of nanofabrication, DNA-directed self-assembly, nanoprinting, plasmonics for sensing and combinatorial photovoltaic materials discovery.